Journal of
Nanoscience and Nanotechnology
Vol. 10, 7362–7365, 2010

Magnetically Tunable Spin Filtering in Semiconductor Nanowires

Ruili Zhang, Jiashu Zhang, Jia Li, Qing Hu, Ruwen Peng*, and Mu Wang

National Laboratory of Solid State Microstructures and Department of Physics, Nanjing University, Nanjing 210093, China

We investigate resonant transmission and spin filtering in symmetric semiconductor nanowires (SSNs), where Rashba spin-orbit coupling (SOC) is symmetrically distributed by applying external electric field. It is shown that electronic bandgap structure has been formed, and the width of the bandgap can be enlarged by increasing the strength of SOC. Resonant transmission has been found in the electronic bandgap, which is characterized by perfect transmission peak. Interestingly, by introducing a weak magnetic modulation, the transmission spectra of spin-up and spin-down electrons are separated. With increasing the length of the centre segment in the SSN, multiple spin-dependent perfect transmission peaks appear in the bandgap. The resonant energy and the number of modes of resonant transmission therein can be manipulated. Around resonant energy, high spin-polarization is observed, and fully spin-polarized conductance is obtained in this SSN. Our investigations achieve potential applications in spin filters.

Keywords: Spin-Polarized Transport, Rashba Spin-Orbit Coupling, Spin Filtering, Spin Injection, Nanowire.

1. INTRODUCTION

In recent years, spin-polarized transport of electrons in semiconductors has attracted intense interest. In semiconductors, spin freedom of electrons can be manipulated efficiently through the mechanism of Rashba spin-orbit coupling (SOC).[1] The strength of the Rashba SOC can be tuned by a gate voltage applied on the semiconductor.[2] When spin-polarized electrons are injected from the ferromagnetic source into the semiconductor channel, one may manipulate the source-to-drain current with the gate voltage. That is the famous Datta-Das spin field-effect transistor (SFET).[3] However, spin injection from the ferromagnetic source into the semiconductor still remains an unsettled issue.[4] Recently, there has been an increased interest in the generation of spin-polarized current out of an unpolarized source. Costa et al.[5] have demonstrated that electrical current flowing through nanowires of ferromagnetic disordered alloys can become highly spin-polarized. A pure spin current and a fully spin-polarized current have been found in a three-terminal spin device.[6] Spin filtering through one-dimensional semiconductor waveguide structures with spatially periodic electric fields has also been reported.[7] For the application of spintronic devices, it is one of the most important problems to understand the mechanism of spin relaxation/dephasing.[8] In recent years, much attention has been devoted to the investigation of spin relaxation in semiconductors.[9–11] By considering all the relevant scattering such as electron–electron, electron–phonon and electron-impurity scattering, Wu et al. have attained a good agreement with the experimental data by Ohno et al.[9, 11] The progress in this field becomes a crucial ingredient in spin-based quantum information processing and semiconductor spintronics.

In this work, we study resonant transmission and spin filtering in symmetric semiconductor nanowires (SSNs), where Rashba spin-orbit coupling (SOC) is symmetrically distributed by applying external electric field. In the Landauer framework of ballistic transport, we have calculated the spin-dependent transmission coefficient, the spin-polarization and the electrical conductance by using the transfer matrix method. It is shown that the spin-dependent electronic bandgap and multiple spin-dependent perfect transmissions in the bandgap have been realized by introducing a weak magnetic potential in the SSNs. Around resonant energy, high spin-polarization is observed, and fully spin-polarized conductance is obtained in this SSN. Our investigations achieve potential applications in spin filters.

2. THE THEORETICAL MODEL

We consider spin-dependent transport of electrons in the symmetric semiconductor nanowire (SSN) constructed as

*Author to whom correspondence should be addressed.

 1533-4880/2010/10/7362/004 doi:10.1166/jnn.2010.2755

$S(m,n)=(BA)^mB^n(AB)^m$, where B and A are the regions with and without Rashba spin-orbit coupling (SOC), respectively, and m and n are the repeating numbers of the units. By this way, a semiconductor superlattice is constructed. In the superlattice, there may exist scattering effects such as electron–electron interaction, electron–phonon and electron-impurity scattering.[11–12] In this work, we investigate how the structure of the superlattice modulates the transport properties of electrons. Then all the scattering aren't included in our present model. Suppose that electron transport along the x-axis in a quasi-one-dimensional waveguide, which is constructed as SSN. The magnetic field is applied in the z-direction and is uniform along the wire. Based on the one-band effective-mass approximation, the Hamiltonian of the system can be written as

$$H=\frac{\hat{p}_x{}^2}{2m^*}+\sigma_z V-\frac{\alpha}{\hbar}\sigma_z\hat{p}_x f(x) \tag{1}$$

where m^* is the effective mass of electrons. In this work, we assume $m^*=0.026\ m_e$, which is reasonable for electrons in the material of InAs.[13] σ_z denotes the spin Pauli matrices, α is the spin-orbit Rashba parameter, and V indicates the strength of the Zeeman-type potential. The function $f(x)$ is introduced to describe the spatial modulations of the SOC, and $f(x)$ equals to 1 and 0 in the regions with and without SOC, respectively.

Due to the fact that the Hamiltonian shown in Eq. (1) is spin diagonal, the electronic eigenstates in the whole system have the form of $|\Psi_\uparrow\rangle=[\psi_\uparrow(x),0]$ and $|\Psi_\downarrow\rangle=[0,\psi_\downarrow(x)]$. In the regions with SOC, the eigenstate has the form of

$$\psi_\sigma^S(x)=C_\sigma^S e^{ik_\sigma^{S1}x}+D_\sigma^S e^{-ik_\sigma^{S2}x} \tag{2}$$

where $\sigma=\uparrow,\downarrow$ indicates spin state of the electron. Here

$$k_\uparrow^{S1}=(\sqrt{2\hbar^2(E-V)/m^*+\alpha^2}+\alpha)m^*/\hbar^2$$
$$k_\uparrow^{S2}=(\sqrt{2\hbar^2(E-V)/m^*+\alpha^2}-\alpha)m^*/\hbar^2$$
$$k_\downarrow^{S1}=(\sqrt{2\hbar^2(E+V)/m^*+\alpha^2}-\alpha)m^*/\hbar^2$$
$$k_\downarrow^{S2}=(\sqrt{2\hbar^2(E+V)/m^*+\alpha^2}+\alpha)m^*/\hbar^2$$

and E is the incident energy of the electron. The eigenstate in the regions without SOC is

$$\psi_\sigma(x)=C_\sigma e^{ik_\sigma^1 x}+D_\sigma e^{-ik_\sigma^2 x} \tag{3}$$

where $k_\sigma^j=k_\sigma^{Sj}(\alpha=0)$, and $j=1,2$. A local coordinate is chosen for each segment, and its origin is positioned at the left-hand side of the segment.[14] Using the continuous conditions, the transfer matrix from B to A layers has the form of

$$M_\sigma^{BA}=\frac{m^*}{\hbar(k_\sigma^1+k_\sigma^2)}\times\begin{pmatrix}\hbar(k_\sigma^2+k_\sigma^{S1})/m^*-\lambda_\sigma\alpha/\hbar & \hbar(k_\sigma^2-k_\sigma^{S2})/m^*-\lambda_\sigma\alpha/\hbar\\ \hbar(k_\sigma^1-k_\sigma^{S1})/m^*+\lambda_\sigma\alpha/\hbar & \hbar(k_\sigma^1+k_\sigma^{S2})/m^*+\lambda_\sigma\alpha/\hbar\end{pmatrix} \tag{4}$$

where $\lambda_{\uparrow,\downarrow}=\pm1$. While the transfer matrix from A to B layers is described as M_σ^{AB}, which can be obtained from Eq. (4) by replacing k_σ^{Sj} with k_σ^j and k_σ^j with k_σ^{Sj}, respectively, and λ_σ is set as $\lambda_{\uparrow,\downarrow}=\mp1$. The electronic propagation within the B layer can be described by matrix M_σ^B,

$$M_\sigma^B=\begin{pmatrix}e^{ik_\sigma^{S1}d} & 0\\ 0 & e^{-ik_\sigma^{S2}d}\end{pmatrix} \tag{5}$$

and the electronic propagation within the A layer can be described by matrix M_σ^A, which can be obtained by replacing k_σ^{Sj} with k_σ^j in Eq. (5). Here $j=1$ and 2. d is the length of one A segment, and one B segment has the same length with one A segment. In the following calculation, d is set as 10 nm. Therefore, the whole system is represented by a product matrix M, relating the incident and reflection waves to the transmission wave. The spin-dependent transmission coefficient T_σ can be obtained through the global transfer matrix M. Then the spin polarization (P) and the total conductance (G)[15] of the system can be achieved by $P=(T_\uparrow-T_\downarrow)/(T_\uparrow+T_\downarrow)$ and $G=(e^2/h)(T_\uparrow+T_\downarrow)$, respectively.

3. THE NUMERICAL CALCULATIONS

Based on the above analysis, we have calculated the spin-dependent transmission coefficient as a function of electron energy in the SSN of $S(m,n)$. As shown in Figure 1, the transmission spectra present several interesting features.

(1) Due to the substructures of "$(BA)^m$" and "$(AB)^m$" in the SSN, there is an electronic bandgap. The width of the bandgap is determined by the strength of SOC. Figures 1(a–c) show the transmission spectra in the SSN of $S(40,2)$ with different α. Here the magnetic potential is set as $V=0$. It is shown that the width of the bandgap can be increased by increasing the strength of SOC.

(2) There exist perfect transmission peak in the electronic bandgap. The quality factor of the resonant peak in the bandgap can be tuned. Figures 1(d–f) present the transmission spectra in the SSN of $S(m,2)$ with different m. The strength of SOC and the magnetic potential are $\alpha=0.10$ a.u. (1a.u. $=1.44\times10^{-9}$ eVm) and $V=0$ mev, respectively. Obviously, the quality factor of the resonant transmission peak in the bandgap is enlarged by increasing m.

(3) The transmission spectra for spin-up and spin-down electrons are separated by introducing a weak magnetic modulation.

Figures 1(g–i) show the transmission coefficients against the electron energy in the SSN of $S(40,2)$ with different magnetic potential, when the strength of SOC is kept as $\alpha=0.10$ a.u. It is shown that the electronic bandgaps for spin-up and spin-down electrons do not coincide with each other when the magnetic potential is introduced. In

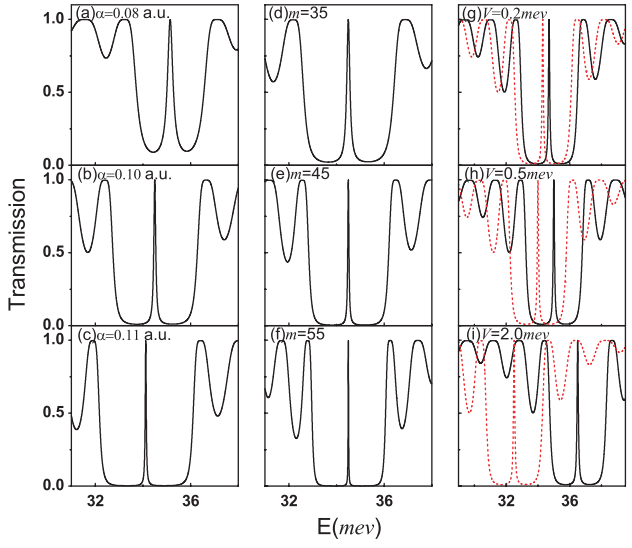

Fig. 1. Figures 1(a)–(c) illustrate the spin-dependent transmission coefficients as a function of the electron energy in the SSN of $S(40, 2)$ with different α, where the magnetic potential is $V = 0$ mev. (a) $\alpha = 0.08$ a.u., (b) $\alpha = 0.10$ a.u., (c) $\alpha = 0.11$ a.u. Figures 1(d)–(f) show the transmission spectra in the SSN of $S(m, 2)$ with different m, where the strength of SOC and the magnetic potential are $\alpha = 0.10$ a.u. and $V = 0$ mev, respectively. (d) $m = 35$, (e) $m = 45$, (f) $m = 55$. And Figures 1(g)–(i) present the transmission spectra in the SSN of $S(40, 2)$ with different magnetic potential, where the strength of SOC is $\alpha = 0.10$ a.u., (g) $V = 0.2$ mev, (h) $V = 0.5$ mev, (i) $V = 2.0$ mev. The black solid line corresponds to spin-up electrons, and the red dashed line corresponds to spin-down electrons.

the bandgap, the resonant energy for spin-up and spin-down electrons are separated. By increasing the magnetic potential, the curves for spin-up and spin-down electrons become farther away from each other. Then the spin-dependent electronic bandgap and the spin-dependent resonant transmission therein are realized.

It is worthwhile to study the spin-dependent resonant transmission in the electronic bandgap for the purpose of application. Figures 2(a–c) show the transmission coefficients against the electron energy in the SSN of $S(40, n)$ with different n. Here the strength of SOC and the magnetic potential are kept as $\alpha = 0.10$ a.u. and $V = 0.10$ mev, respectively. Obviously, the central part "B^n" determines the peak number and the energy of perfect transmission peaks in the bandgap for each spin state of electrons. We find that more and more perfect transmission peaks for spin-up or spin-down electrons appear in the bandgap by increasing n. For example, there is one peak for spin-up or spin-down electrons in the bandgap when $n = 2$ (as shown in Fig. 2(a)). There are two peaks for spin-up or spin-down electrons in the bandgap when $n = 40$ (as shown in Fig. 2(b)). And three peaks for spin-up or spin-down electrons appear in the bandgap when $n = 80$ (as shown in Fig. 2(c)). This feature originates from the fact that the reflected wave at each interface has changed its phase when n increases. Once the phase difference of the reflected waves becomes an integer multiple of π, the total reflected waves at the interface reaches zero due to interference. As a result, more transmission peaks lie in the bandgap by increasing the length of the central segment B^n in SSN of $S(40, n)$. Moreover, the magnetic potential can modulate the wave vectors of spin-up and spin-down electrons differently. Therefore, the resonant transmissions in the bandgap are spin-dependent. These features may have potential applications in the designing of spin filters.

We can tune the spin-polarization by changing both the electron energy and the length of the centre segment B^n in SSN. Figures 2(d–f) present the spin-polarization against the electron energy in SSN of $S(40, n)$ with different n. Obviously, the spin-polarization can be changed alternatively from positive to negative when the electron energy is varied. Around resonant energy, high spin-polarization has been observed and the spin-polarization has been reversed. This feature originates from the fact that resonant energies are spin-dependent (as shown in Figs. 2(a–c)). On the other hand, because more and more spin-dependent transmission peaks appear by increasing n in the SSN, multiple reversals of spin-polarization happen in the bandgap. Consequently, the spin-polarization reversal and the reversal times for tunneling electrons can be modulated by tuning the length of the centre segment B^n in the SSN of $S(40, n)$.

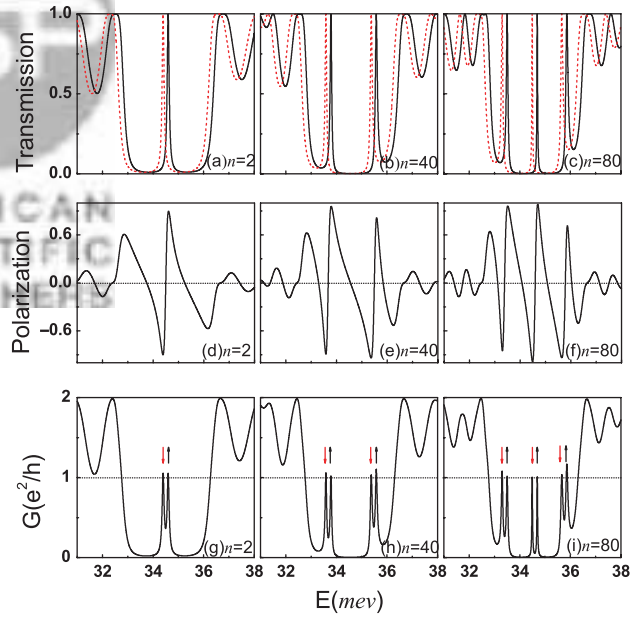

Fig. 2. The spin-dependent transmission coefficients, the spin-polarization, and the conductance (G) as a function of the electron energy in the SSN of $S(40, n)$ with different n, respectively. Here the strength of SOC and the magnetic potential are $\alpha = 0.10$ a.u. and $V = 0.10$ mev, respectively. For transmission coefficients: (a) $n = 2$, (b) $n = 40$, and (c) $n = 80$. The black solid line corresponds to spin-up electrons, and the red dashed line corresponds to spin-down electrons. For the spin-polarization: (d) $n = 2$, (e) $n = 40$, and (f) $n = 80$. And for the conductance: (g) $n = 2$, (h) $n = 40$, and (i) $n = 80$, where the arrow implies the conductance peak contributed by spin-up (↑) or spin-down (↓) electrons.

The electrical conductance of the SSN can also be obtained. As shown in Figures 2(g)–(i), there exist conductance peaks within the bandgap against the electron energy in the SSNs of $S(40, n)$ with different n. The electrical conductance within the bandgap is about e^2/h at each resonant energy. As we have known, resonant energies are spin-dependent. At the resonant energy of spin-up electron, the transmission for spin-down electron is close to zero. While at the resonant energy of spin-down electron, the transmission for spin-up electron is almost zero (as shown in Figs. 2(a–c)). As a result, the electrical conductance around the resonant energy comes mainly from one kind of spin electrons. Then fully spin-polarized conductance with the value of e^2/h can be observed within the bandgap. On the other hand, more and more peaks with about e^2/h appear in the bandgap when n increases (as shown in Figs. 2(g–i)). Interestingly, the conductance peaks contributed by spin-up and spin-down electrons appear alternately in the bandgap. For instance, the $(2i-1)$th conductance peak mainly comes from the spin-down electron, and the $(2i)$th conductance peak mainly comes from the spin-up electron in the SSN of $S(40, n)$. Here $i = 1$ in the case of $S(40, 2)$ (as shown in Fig. 2(g)), $i = 2$ in the case of $S(40, 40)$ (as shown in Fig. 2(h)), $i = 3$ in the case of $S(40, 80)$ (as shown in Fig. 2(i)). From this point of view, it is possible to use the SSNs to generate spin-polarized current out of an unpolarized source and perform as spin filtering.

4. SUMMARY

In summary, we have studied resonant transmission and spin filtering in SSNs, where SOC is symmetrically distributed by applying external electric field. It is shown that electronic bandgap structure has been formed, and the width of the bandgap can be increased by increasing the strength of SOC. Due to the internal symmetry of the SSN, there exist perfect transmission peak in the electronic bandgap. By introducing a weak magnetic modulation, the transmission spectra of spinup and spindown electrons are separated. When the length of the centre segment in the SSN is increased, multiple spin-dependent perfect transmissions occur in the electronic bandgap. Around resonant energy, high spin-polarization is observed, and fully spin-polarized conductance is obtained in this SSN. Our investigations achieve potential applications in spin filters.

Acknowledgments: This work was supported by grants from the National Natural Science Foundation of China (Grant Nos. 10625417, 50672035, 10874068, and 10904061), the State Key Program for Basic Research from the Ministry of Science and Technology of China (Grant Nos. 2004CB619005 and 2006CB921804), and partly by Jiangsu Province (Grant No. BK2008012).

References and Notes

1. E. I. Rashba, *Sov. Phys. Solid State* 2, 1190 (**1960**).
2. J. Nitta, T. Akazaki, H. Takayanagi, and T. Enoki, *Phys. Rev. Lett.* 78, 1335 (**1997**); D. Grundler, *Phys. Rev. Lett.* 84, 6074 (**2000**).
3. S. Datta and B. Das, *Appl. Phys. Lett.* 56, 665 (**1990**).
4. S. A. Wolf, D. D. Awschalom, R. A. Buhrman, J. M. Daughton, S. von Molnár, M. L. Roukes, A. Y. Chtchelkanova, and D. M. Treger, *Science* 294, 1488 (**2001**); G. Schmidt, D. Ferrand, L. W. Molenkamp, A. T. Filip, and B. J. Van Wees, *Phys. Rev. B* 62, 4790(R) (**2000**).
5. A. T. Costa, Jr. and R. B. Muniz, *Phys. Rev. B* 66, 113402 (**2002**).
6. H.-F. Lü and Y. Guo, *Appl. Phys. Lett.* 91, 092128 (**2007**).
7. S. J. Gong and Z. Q. Yang, *J. Appl. Phys.* 102, 033706 (**2007**); L. G. Wang, K. Chang, and K. S. Chan, *J. Appl. Phys.* 99, 043701 (**2006**).
8. I. Zutic, J. Fabian, and S. Das Sarma, *Rev. Mod. Phys.* 76, 323 (**2004**).
9. Y. Ohno, R. Terauchi, T. Adachi, F. Matsukura, and H. Ohno, *Phys. Rev. Lett.* 83, 4196 (**1999**); Y. Ohno, R. Terauchi, T. Adachi, F. Matsukura, and H. Ohno, *Physica E*, (Amsterdam) 6, 817 (**2000**).
10. J. Zhou and M. W. Wu, *Phys. Rev. B* 77, 075318 (**2008**).
11. J. Zhou, J. L. Cheng, and M. W. Wu, *Phys. Rev. B* 75, 045305 (**2007**).
12. M. Q. Weng, M. W. Wu, and L. Jiang, *Phys. Rev. B* 69, 245320 (**2004**).
13. I. Vurgaftman, J. R. Meyer, and L. R. Ram-Mohan, *J. Appl. Phys.* 89, 5815 (**2001**); Y. Lacroix, C. A. Tran, S. P. Watkins, and M. L. W. Thewalt, *J. Appl. Phys.* 80, 6416 (**1996**).
14. R. L. Zhang, Z. J. Zhang, R. W. Peng, X. Wu, D. Li, J. Li, and L. S. Cao, *J. Appl. Phys.* 103, 07B727 (**2008**).
15. K. M. Jiang, Z. M. Zheng, B. G. Wang, and D. Y. Xing, *Appl. Phys. Lett.* 89, 012105 (**2006**); Y. Imry and R. Landauer, *Rev. Mod. Phys.* 71, S306 (**1999**).

Received: 4 September 2009. Accepted: 30 October 2009.